# Deformation of a droplet in an electrical field: Transient response in dielectric media.

Graeme Supeene, Charles R. Koch and Subir Bhattacharjee*
Department of Mechanical Engineering,
4-9 Mechanical Engineering Building.,
University of Alberta, Edmonton, AB, T6G 2G8, Canada.

October 12, 2004

**Abstract**

Deformation of droplets in an externally imposed electrical field is a widely studied phenomenon, and is an important component of microfluidic operations involving electrical actuation of droplets. The ability to control deformation of a droplet provides the ability to manipulate these droplets in a controlled manner on a microfluidic chip. In this study, we explore a general mathematical formulation for the deformation of droplets under an imposed electrical field. The coupled fluid mechanical and electrostatic governing equations are solved numerically using finite element analysis, and the solution is presented for two perfect dielectrics carrying no free charge. The numerical solutions are first compared with an asymptotic analytic result to assess the accuracy of the numerical code. Following this, the dynamics of the deformation are presented to characterize the typical response of a droplet subjected to a step change in the electric field. The results provide a basis for modeling the dynamic response and formulating control strategies for droplet manipulation, and may provide considerable insight into microfluidic operations based on electrowetting.

**Keywords:** Droplet deformation; Electric field; Laplace equation; Navier-Stokes equations; Finite element; System identification.

*Corresponding Author: Tel: (780) 492 6712; Fax: (780) 492 2200; Email: Subir.B@ualberta.ca

# 1 Introduction

A liquid droplet suspended in an immiscible medium having different dielectric properties will deform under the influence of an applied electric field. This deformation was first described by O'Konski and Thacher [1], and later by Allan and Mason [2], who assumed that both fluids were perfect dielectrics carrying no free charge (zero conductivity). Their theory, which is based on linearization about a spherical initial shape, predicts that the steady-state droplet shape will always be a prolate spheroid with its polar axis aligned parallel to the electric field. The steady state involves no fluid motion, since the electrical stress occurs only at the droplet boundary and is normal to it. Using small perturbations in the parameters caused by the application of a low-intensity electric field $\delta\vec{E}$, the O'Konski & Thacher/Allan & Mason (OTAM) result predicts a deformation of the following form:

$$\frac{\delta d_{OTAM}}{\delta W} = \frac{9(S-1)^2}{16(S+2)^2} \tag{1}$$

where the deformation parameter $d_{OTAM}$ is defined as:

$$d_{OTAM} = \frac{b-a}{b+a} \tag{2}$$

in which $b$ is the polar radius of the spheroid and $a$ is the equatorial radius, as shown in Figure 1. The parameter $\delta W$ contains the absolute dependence of the deformation on the physical parameters, and is defined as:

$$\delta W = \frac{\epsilon_0 \epsilon_e a}{\gamma} \delta E^2 \tag{3}$$

where $\epsilon_0$ is the permittivity of vacuum, $\epsilon_e$ is the dielectric constant of the external fluid and $\gamma$ is the interfacial tension. The parameter $S$ in Eq. (1) is the ratio of dielectric permittivities of the two fluids:

$$S = \frac{\epsilon_i}{\epsilon_e} \tag{4}$$

The objective of this paper is to address the problem of deformation of a perfectly dielectric droplet in another dielectric medium, for which Eq. (1) represents the equilibrium deformation under the influence of an external electric field. First, a brief overview of the theoretical and experimental developments in this area is presented.

The experiments of Allan & Mason [2] did not agree with their theory well, and in fact showed that the deformed shape could be an oblate spheroid in some cases (the axis along the applied field being shortened). This phenomenon has since been noted by

other researchers [3-6]. Taylor [7], recognizing that the assumption of zero conductivity is not representative of realistic conditions, formulated an alternative theory based on the fluids having free or mobile charges – leading to what is called the "leaky dielectric" model. In this model, the fluids contain free ions which migrate under the influence of the electric field, building up on the boundary of the droplet and allowing tangential electrical stresses to develop. The Taylor result predicts a deformation of the form:

$$\frac{\delta d_{Taylor}}{\delta W} = \frac{9}{16(H+2)^2}\left[1 + H^2 - 2S + \frac{3}{5}(H-S)\frac{2+3M}{1+M}\right] \tag{5}$$

which contains two additional parameters, $H$ the conductivity ratio and $M$ the viscosity ratio of the internal to external fluids:

$$H = \frac{\sigma_i}{\sigma_e}, \qquad M = \frac{\mu_i}{\mu_e} \tag{6}$$

In contrast to the OTAM result, Taylor's model can predict oblate deformation under certain circumstances and it shows better qualitative agreement with experiments. However, one cannot recover the OTAM result by setting both fluid conductivities to zero in the Taylor result, since the latter depends not on the absolute values of the conductivities but only on their ratio. This indicates that the leaky dielectric theory used in Taylor's model is not sufficiently general.

The Taylor theory assumes that ion diffusion in both fluids is insignificant, so that ion buildup occurs in a vanishingly thin layer at the drop interface. If diffusion effects are significant, the Taylor theory is inadequate. Recently, Zholkovskij *et al.* [8] proposed an electrokinetic model which takes into account diffusion effects, thus bridging the gap between the OTAM and Taylor theories. This electrokinetic theory varies monotonically between the perfect and leaky dielectric theories based on the thickness of the electrostatic double layer relative to the droplet diameter.

All of these analytical results are steady-state analyses based on the assumption that deformations are small, and that the deformed shape is spheroidal. The resulting expression for the electrokinetic model is nevertheless extremely complex. The underlying physical problem exhibits nonlinear behaviour, including non-spheroidal shapes at larger deformations [2,9-11]. In addition, time dependence increases the complexity of the problem dramatically. Further analytic work may well be possible, but in order to analyze the transient behaviour of these droplets, or to extend the theory to large deformations, numerical methods seem better suited. The boundary integral method has been employed [9] to analyze large deformations and breakup of drops near equilibrium. The finite element method has been used in a steady-state analysis of the leaky

dielectric (Taylor) model with large deformations [10], and in a full dynamic analysis of the same using a steady applied electric field [11].

The present work is a finite element analysis of the dynamic behaviour of a droplet when a uniform electric field is set up. As a preliminary to the analysis of the full electrokinetic problem, the limit at zero conductivity has been described in this paper. The methodology presented here addresses the dynamic response of a droplet in a uniform electric field, leading to a numerical analogue of the OTAM result at steady state. However, the numerical model is capable of predicting large-scale nonlinear deformations of the droplet, as well as the transient response of the droplet subject to a step change in the electric field.

The purpose of this analysis is to observe the effects of electric field intensity, interfacial tension, and fluid viscosity variation on the dynamic response of a suspended droplet. This knowledge may be of use in the field of microfluidic actuation mechanisms employed in lab-on-a-chip devices. More specifically, the transient response of the droplets under an imposed electrical field is of immense interest in developing actuation techniques based on electrowetting (EW) or electrowetting on a dielectric (EWOD) phenomena [12, 13]. In these techniques, micron-scale fluid droplets are rapidly transported around a microchip on electrode paths. The dynamic behaviour and control of the movement of such droplets is an area of great interest.

# 2 Theory

Figure 1 shows the system under consideration. It is assumed that the geometry remains axially symmetric. The mathematical problem consists of a system of coupled electrical and fluid mechanical equations, with appropriate boundary conditions at infinity and at the interface between the two fluids. The present analysis will be restricted to the problem of deformation of perfect dielectrics containing no mobile or free charge. This eliminates the need for an equation describing the free charge distribution.

The deformation of the drop results from a balance of Maxwell electric stress, viscous fluid stress, and surface tension at the interface between the two fluids. In the case of perfect dielectric fluids, the viscous stresses only affect the transient behaviour, since the system is quiescent at equilibrium. The stress balance can be represented

as [8]:

$$\frac{\epsilon_0}{2}\{\epsilon_e(\nabla\Psi_e\cdot\hat{n})^2-\epsilon_i(\nabla\Psi_i\cdot\hat{n})^2-(\epsilon_e-\epsilon_i)[(\nabla\Psi_i)^2-(\nabla\Psi_i\cdot\hat{n})^2]\}$$
$$-(P_e-P_i)+\{\mu_e[\nabla\vec{U}_e+(\nabla\vec{U}_e)^T]\cdot\hat{n}-\mu_i[\nabla\vec{U}_i+(\nabla\vec{U}_i)^T]\cdot\hat{n}\}\cdot\hat{n}=2\gamma X \quad (7)$$

Here, $\Psi$ is the electric potential, $\vec{U}$ is the velocity vector, $P$ is the pressure, $\gamma$ is the interfacial tension, and $X$ is the local mean curvature of the interface. The unit normal $\hat{n}$ points outward from the drop interface into the medium. The superscript $^T$ indicates the transpose of a tensor, while the subscripts $_i$ and $_e$ represent the internal and external fluids, respectively.

The first term in Eq. (7) is the normal component of the Maxwell electrical stress on the boundary. The tangential stress is zero, since there is no free charge buildup on the interface itself. This remains true even in the general electrokinetic model, where the free charge distribution is a volume effect rather than a surface phenomenon. The second and third terms represent the pressure difference across the interface and the normal contribution of the fluid stresses respectively. The right hand side describes the normally directed resultant of the interfacial tension in the curved drop boundary, assuming that $\gamma$ is uniform and constant. The shape of the droplet can be derived by integrating the surface mean curvature $X$. The electric potential, pressure distribution, and velocity field must be known in order to do this.

## 2.1 Electrostatic Model

The electric potential in the perfect dielectric problem is described by the Laplace equation,

$$\nabla^2\Psi=0 \quad (8)$$

subject to boundary conditions representing uniform electric field far from the drop, and continuity of electric potential and electric displacement at the drop interface:

$$\nabla\Psi=-\vec{E} \quad \text{at infinity} \quad (9)$$

$$\Psi_i=\Psi_e \quad \text{at interface} \quad (10)$$

and

$$(\epsilon_e\nabla\Psi_e-\epsilon_i\nabla\Psi_i)\cdot\hat{n}=0 \quad \text{at interface} \quad (11)$$

We assume that the electrostatic system responds instantaneously to any changes in geometry caused by deformation of the drop.

## 2.2 Fluid Mechanical Model

In order to maintain generality for high electric fields and interfacial tension values, the full incompressible Navier-Stokes equations were employed:

$$\rho\frac{\partial\vec{v}}{\partial t} - \nabla\cdot\mu(\nabla\vec{v} + (\nabla\vec{v})^T) + \rho(\vec{v}\cdot\nabla)\vec{v} + \nabla P = 0 \quad (momentum) \tag{12}$$

along with the continuity equation for incompressible fluids

$$\nabla\cdot\vec{v} = 0 \qquad (continuity) \tag{13}$$

Here, the zero on the right hand side of the momentum equation (Eq. 12) indicates that there is no net body force acting on the fluid bulk. In all cases gravity has been assumed to be negligible.

The boundary conditions for the fluid dynamics problem reflect quiescence at infinity and continuity at the boundary:

$$\vec{v} = 0 \quad \text{at infinity} \tag{14}$$

$$P = 0 \quad \text{at infinity} \tag{15}$$

$$\vec{v}_i = \vec{v}_e = \vec{v}_{interface} \quad \text{at interface} \tag{16}$$

$$\{\mu_e[\nabla\vec{U}_e + (\nabla\vec{U}_e)^T]\cdot\hat{n} - \mu_i[\nabla\vec{U}_i + (\nabla\vec{U}_i)^T]\cdot\hat{n}\}\times\hat{n} = 0 \quad \text{at interface} \tag{17}$$

The last condition, Eq. (17), represents continuity of tangential viscous stresses.

The solution of these coupled systems of equations, combined with the boundary condition in Eq. (7), yields a time-domain solution for the deformation of a perfect dielectric fluid droplet in an immiscible perfect dielectric medium.

## 2.3 Dynamic Analysis of the Drop

To facilitate generation of time response histories of droplet deformation to an arbitrarily changing electric field strength with modest amounts of computational burden, a lumped parameter model of the system is used. A lumped parameter (LP) model of the drop is an ordinary differential equation which facilitates prediction of system performance without the computational burden of FEA. The LP model will be shown to

provide reliable response trajectories once it is parameterized using static and transient FEA results.

The drop deformation $d$ is nondimensionalized by its equilibrium value at the OTAM limit, and time $t$ by a characteristic system time. The drop deformation is normalized as

$$\bar{d} = \frac{d}{d_{OTAM}} \tag{18}$$

where $d_{OTAM}$ is the steady-state deformation at the OTAM limit, calculated from Eq. (1). The time is normalized by the inviscid natural frequency [14], given by

$$f_0 = \frac{1}{2\pi}\sqrt{\frac{24\gamma}{(2\rho_e + 3\rho_i)a^3}} \tag{19}$$

where $a$ is the initial radius of the spherical drop, yielding

$$\bar{t} = tf_0 \tag{20}$$

Parametric system identification on the normalized time and drop diameter is used to obtain a simple LP model of the dynamics of the drop distortion to a step input in the electric field strength. Here a second order ARMAX (AutoRegressive Moving Average eXtra input) [15] model was found to sufficiently characterize the input-output response of the FEA model. The discrete time second order ARMAX model is then converted to a continuous equivalent system which results in a continuous transfer function of the form

$$\frac{\bar{d}}{\bar{E}} = \frac{1}{s^2 + 2\zeta\omega_n s + \omega_n^2} \tag{21}$$

where $\bar{d}$ is the normalized drop distortion, $\omega_n$ and $\zeta$ are the natural frequency and damping ratio, respectively, and $\bar{E}$ is the normalized electric field. The electric field is normalized by the same value of $E$ used to compute the OTAM limit for the normalization of $d$.

# 3 Numerical Solution

## 3.1 Discrete Problem Formulation

Discretization of the governing system of equations outlined in Section 2 was performed using the finite element method. The primary advantages of the technique are the ability to adaptively size the mesh to conform to the changing geometry of the problem

at the curved boundary of the deforming droplet, as well as its suitability for use with the nonlinear Navier-Stokes equations. The formulation was implemented using a MATLAB-compatible commercial software package called FEMLAB [16].

The model consists of two problems, one for the fluid mechanics and one for the electrostatics, which are solved in a segregated manner. Each problem is solved in two subdomains, representing the drop and the continuous phase. The meshed geometry is shown in Figure 2. The computational domain is a square, with side length equal to ten drop radii, and a plane of symmetry is employed at the drop equator in order to prevent drifting of the droplet. The domains are discretized into triangular elements using a Delaunay algorithm with refinement near the drop interface. All simulations were run with 4029 nodes on 1970 elements in the fluid problem, and 19447 nodes on 4272 elements in the electrostatic problem.

The velocity field is discretized using quadratic Lagrange elements, and the pressure field using linear Lagrange elements. In order to allow for the presence of a pressure discontinuity at the interface, separate problem definitions are used for the two fluid phases. Coupling between the two fluids is achieved by specifying continuity of velocity in addition to the defined pressure difference of Eq. (7). The electric potential is discretized using cubic Lagrange elements, because of the importance of obtaining an accurate first derivative. The electric stress on the droplet boundary depends on the square of the electric field.

The simulations are performed to track the transient deformation of an initially spherical drop subject to a step application of a uniform electric field. First, the linear time-invariant electrostatic problem is solved, and its solution is used to construct the boundary condition for the drop interface in the Navier-Stokes problem. The nonlinear time-dependent fluid mechanics problem is then solved for a given time step, using the FEMLAB time-dependent solver framework `femtime` with the variable-order ODE solver `fldaspk` [16]. The velocity and pressure fields are determined at the beginning, middle, and end of each time step. After solution of the fluid mechanics problem, the mesh is moved based on a quadratic velocity average over the time step, as follows:

$$\vec{x}(t+\Delta t) = \vec{x}(t) + \Delta t \left[ \frac{1}{6}\vec{v}(t) + \frac{2}{3}\vec{v}(t+\frac{\Delta t}{2}) + \frac{1}{6}\vec{v}(t+\Delta t) \right] \tag{22}$$

where $\vec{x}$ is the position of each mesh point, and $\vec{v}$ is the corresponding velocity vector. The initial condition for the fluid problem in any given time step is the final solution from the previous time step, interpolated to the new node positions.

Since the finite elements deform as the fluid moves, it might be expected that they

would become unacceptably strained at some point, requiring a remeshing over the geometry to restore element quality. The code developed here will perform a remesh if the element quality becomes too low, but this did not occur while simulating the relatively small deformations presented here.

## 3.2 Convergence Testing

To assess the sensitivity of the simulation results to the mesh and the time steps, a series of simulations were conducted with varying degrees of mesh refinement and different timestepping algorithms and time steps.

Figure 3 shows the effect of grid refinement in the fluid mechanics problem. Here, the transient deformation over a time range from 0.2 to 1 $\mu$s is depicted for different values of the mesh control parameters. The horizontal dashed line in the figure represents the steady-state deformation based on the OTAM result. Two parameters in the FEMLAB function `meshinit` are used to specify the mesh, namely `Hcurve` and `Hgrad`. The first is a multiplier that determines local refinement based on boundary curvature. The second describes the rate of growth of element size away from such a region of local refinement. It may be seen from Figure 3 that `Hcurve` has a significant effect on the convergence of the solution, and that the solution is essentially converged at a value of 0.03. This corresponds to a resolution of 54 vertices (107 nodes) along the length of the interfacial boundary. On the other hand, the mesh growth factor `Hgrad` has no significant effect, implying that the mesh further away from the boundary is much less important, and hence that a general refinement would be of limited value.

Figure 4 shows the effect of time step refinement on the transient deformation. The time step used in the base case was 5 nanoseconds. It may be seen that the error introduced by the time discretization using steps ranging from 10 to 2 ns is on the order of 0.5% at the peak of the curve. Errors of similar magnitude are obtained for the case of highest electric field and lowest viscosity employed in our simulations, with an appropriate time step. It should be noted that use of larger time steps is desired to accelerate the attainment of the steady state. For this, a nonuniform timestepping technique might be pertinent. However, although certain elementary techniques were found to be fairly adequate for the transient oscillatory parts of the deformation, these techniques resulted in instabilities at the later stages of the simulation. Consequently, all our simulations use a uniform time step.

Typically, the dynamic analyses for smaller deformations converge to within 0.2% of the analytic OTAM limit for the steady state deformation.

Table 1: Parameters for the simulations.

| | |
|---|---|
| Applied Electric Field $E$ | 1 MV/m |
| Droplet Radius $a$ | 1 $\mu$m |
| Droplet Relative Permittivity $\epsilon_i$ | 80 |
| Medium Relative Permittivity $\epsilon_e$ | 3 |
| Interfacial Tension $\gamma$ | 30 mJ/m$^2$ |
| Droplet Density $\rho_i$ | 1000 kg/m$^3$ |
| Medium Density $\rho_e$ | 1000 kg/m$^3$ |
| Droplet Viscosity $\mu_i$ | 0.001 Pa·s |
| Medium Viscosity $\mu_e$ | 0.001 Pa·s |

Table 2: Range of Parameters used in the simulations.

| | |
|---|---|
| Applied Electric Field $E$ | 333 kV/m - 3 MV/m |
| Interfacial Tension $\gamma$ | 10 - 70 mJ/m$^2$ |
| Droplet Viscosity $\mu_i$ | 0.0001 - 0.01 Pa·s |
| Medium Viscosity $\mu_e$ | 0.0001 - 0.01 Pa·s |

# 4 Results and Discussion

Simulations of droplet dynamic response to an applied electric field step input were conducted over a parameter space encompassing a range of fluid properties characteristic of common liquids, with applied electric fields low enough to keep deformations small. The typical parameter values for the simulations are listed in Table 1. We refer to these parameters as the baseline case, and vary some of these parameters, such as electric field strength, interfacial tension, and the viscosities of the fluids, to assess their influence on the deformation with respect to the deformation obtained in the baseline simulation. The densities, relative permittivities, and droplet radius were not varied. The range of values over which the other parameters were varied is shown in Table 2.

In the following, we depict the influence of the electric field strength, interfacial tension, and fluid viscosities on the dynamic response of a droplet.

## 4.1 Effect of Field Strength

Analytic steady-state results include a dependency of the deformation on the square of the applied field, $E^2$. It is expected that this dependency should appear in low-deformation numerical simulations as well. It is also expected that if the dynamic response of the drop is nearly linear at these values of deformation, it should be possible to collapse the step responses at various field strengths onto a single curve with an appropriate nondimensionalization. The nondimensionalization implemented here scales $d$ by its equilibrium value at the OTAM limit ($d_{OTAM}$), and $t$ by a characteristic system frequency. The nondimensional deformation given by Eq. (18) is plotted against the nondimensional time, Eq. (20), in Figure 5 for different values of the imposed electric field strength. The step responses do indeed almost exactly collapse onto a single curve converging to a steady state value of very near unity. Only the highest applied field strength of 3 MV/m shows a slight offset. This indicates that the physics of the problem is being accurately captured in the simulations, and that we can proceed with confidence in further analyses involving small equilibrium deformations.

The transient behaviour of the deformation is oscillatory, with over and undershoot in the deformation curves indicating an under-damped system response. All the curves converge to the same steady state deformation obtained analytically in the OTAM limit, Eq. (1). As mentioned earlier, the numerical predictions generally converged to within 0.2% of the corresponding steady-state deformations predicted by the analytical expression, Eq. (1).

## 4.2 Effect of Interfacial Tension

Figure 6 shows the variation of the normalized deformation with scaled time for different values of the interfacial tension. The simulations are performed by keeping all other parameters fixed at the values given in Table 1. Over the range of interfacial tensions studied, the droplet deformation is always underdamped, and has two peaks. The steady state deformations all converge to the OTAM limit deformation, Eq. (1). A closer inspection of the first peak in the transient curves indicates that increasing the interfacial tension increases the overshoot. The position of the first peak also shifts slightly to the left, which is typical of a linear underdamped second order system. The undershoot is substantially smaller, and is almost imperceptible at the lowest interfacial tension of 20 mJ/m$^2$.

System identification on the finite element model generated step response is performed to obtain the parametric model parameters. Statistically, a second order AR-

MAX model is found to provide an acceptable trade-off between model complexity and error in the model fit. This second order model provides the natural frequency and the damping ratio which vary as the physical parameters of the system are varied. For example, varying interfacial tension changes the identified natural frequency and damping ratio as depicted in Figure 7. Increasing interfacial tension causes the damping ratio to decrease and the natural frequency to increase, indicating that the droplet becomes "stiffer". The equilibrium deformation parameter is also reduced, although this effect as well as most of the increase in natural frequency is masked by the normalization of the data.

## 4.3 Effect of Viscosity

The viscosities of the fluids do not appear in the steady-state analysis of the problem since fluid flow is not involved. However, viscosity plays a key role in the dynamic evolution of the droplet shape under the imposed electric field. Variations in the absolute values of the viscosities and in the ratio between them result in changes to both the Navier-Stokes solution as a whole and the resultant stress on the interface. Here, the effects of viscosity on the dynamic response of the droplet are discussed.

The effect of viscosity ratio on the dynamic response of the droplet is shown in Figure 8, which is obtained by varying the viscosity ratio while keeping the maximum viscosity fixed at 0.001 Pa·s. The maximum viscosity is assigned to either of the fluids (droplet or external medium) to explore a range of ratios. For instance, setting the viscosity of the external fluid, $\mu_e$, to 0.001 Pa·s, one obtains the viscosity of the internal fluid to be $\mu_i = 0.0001$ Pa·s for a viscosity ratio $\mu_i/\mu_e$ of 0.1. On the other hand, setting $\mu_i = 0.001$ Pa·s, we obtain $\mu_e = 0.0001$ Pa·s for $\mu_i/\mu_e = 10$. This allows exploration of a wide range of viscosity ratios ranging from 0.1 to 10.

The influence of the viscosity ratio on the droplet deformation dynamics is quite substantial. For all other values of the viscosity ratio except 1, the nature of the dynamic response is significantly different. When $\mu_i/\mu_e$ is 1, the response curve has two visible peaks. For all other viscosity ratios, the response curves appear to have a third oscillatory peak. Comparing the curves for viscosity ratios $> 1$ against those $< 1$, we note that a reduced external fluid viscosity will render the dynamic response more underdamped. The peaks in the oscillation will be larger for these cases. This behaviour is apparent in the plots of the natural frequency and the damping ratio shown in Figure 9. We observe that the natural frequency has a minimum value for a viscosity ratio of 1, and it increases as the viscosity ratio is either decreased or increased. Furthermore, the increase in the natural frequency is more pronounced for

viscosity ratios $< 1$. The damping ratio is the highest for a viscosity ratio of 1. For other values of the viscosity ratio, the damping ratio decreases. Once again, viscosity ratios $< 1$ have a greater influence on the damping ratio.

To observe the effect of the viscosities on the dynamic response, simulations were performed by changing the viscosities of the droplet and the medium while keeping their ratio fixed at 1. Figure 10 shows the dynamic response of the droplet for these cases. It is evident that while the system is underdamped for the lowest viscosity, it becomes nearly overdamped when the viscosity is increased by a factor of only 2.5. In the case of higher viscosities, the droplet deformation becomes overdamped and monotonic. The dynamic response of the fluid droplet is significantly affected when the viscosities of both the fluids are changed simultaneously.

The influence of the viscosities on the natural frequency and damping ratio can be seen in Figure 11. While the natural frequency is not significantly affected by the increase in viscosity, the damping ratio increases dramatically. The system becomes overdamped above viscosities of 0.003 Pa·s. Highly viscous systems will have a slower and a monotonic transition to the steady state deformation.

## 4.4 Significance of the lumped parameter model

The lumped parameter (LP) model obtained by fitting only two parameters, the damping ratio, $\zeta$, and the natural frequency, $\omega_n$, provides considerable insight into the dynamic response of the droplet and enables development of control strategies for actuating the droplets. The transfer function in Eq. (21) provides a facile means of expressing the dynamic response of a droplet under an external field and captures the essential details of the entire time evolution of the droplet deformation. Such a model, provided the natural frequencies and the damping ratios are appropriately correlated with the operating variables, can provide a dynamic response rapidly, and can be implemented in real time control strategies. Using the LP model, an arbitrary electric field strength can be input at each time step of the droplet deformation and the resulting model dynamics can be, with minimal computational burden, propagated forward in time. This is in contrast to the FEA model which requires a substantial amount of computation for each simulation. The existence of a simple LP model is expedient for both closed control law design and subsequent simulation testing of the control law performance. Here the LP model could be used to design feedback based on drop deformation while using the electric field strength as the system input.

# 5 Concluding Remarks

A finite element analysis of the transient problem involving the deformation of a perfect dielectric droplet in a uniform electric field is presented. The simulations provide considerable insight regarding the influence of the interfacial tension and viscosity on the evolution of the droplet shape with time. In particular, the combined influence of the two fluid viscosities is not apparent in the classical treatments of this problem. A simple second order linear transfer function captures the essential features of the dynamic response of the droplet through two adjustable parameters, namely, the natural frequency and the damping ratio. This lumped parameter representation of the droplet's response to an electrical actuation might be useful in development of control strategies for droplet actuation in microfluidic devices.

# 6 Acknowledgments

The authors acknowledge financial support for this research from National Sciences and Engineering Research Council of Canada (NSERC).

# References

[1] C. T. O'Konski and H. C. Thacher. The distortion of aerosol droplets by an electric field. *J. Phys. Chem.*, 57:955–958, 1953.

[2] R. S. Allan and S. G. Mason. Particle behaviour in shear and electric fields .1. deformation and burst of fluid drops. *Proc. Roy. Soc. Lond. A-Math. Phys. Sci.*, 267(1328):45–61, 1962.

[3] S. Torza, R. G. Cox, and S. G. Mason. Electrohydrodynamic deformation and burst of liquid drops. *Phil. Trans. Roy. Soc. Lond. A-Math. Phys. Sci.*, 269(1198):295–319, 1971.

[4] P. A. Arp, R. T. Foister, and S. G. Mason. Some electrohydrodynamic effects in fluid dispersions. *Adv. Colloid Interf. Sci.*, 12(4):295–356, 1980.

[5] O. Vizika and D. A. Saville. The electrohydrodynamic deformation of drops suspended in liquids in steady and oscillatory electric-fields. *J. Fluid Mech.*, 239:1–21, 1992.

[6] J. W. Ha and S. M. Yang. Effects of surfactant on the deformation and stability of a drop in a viscous-fluid in an electric-field. *J. Colloid Interf. Sci.*, 175(2):369–385, 1995.

[7] G. Taylor. Studies in electrohydrodynamics .i. circulation produced in a drop by an electric field. *Proc. Roy. Soc. Lond. A-Math. Phys. Sci.*, 291(1425):159–166, 1966.

[8] E. K. Zholkovskij, J. H. Masliyah, and J. Czarnecki. An electrokinetic model of drop deformation in an electric field. *J. Fluid Mech.*, 472:1–27, 2002.

[9] J. D. Sherwood. Breakup of fluid droplets in electric and magnetic-fields. *J. Fluid Mech.*, 188:133–146, 1988.

[10] J. Q. Feng and T. C. Scott. A computational analysis of electrohydrodynamics of a leaky dielectric drop in an electric field. *J. Fluid Mech.*, 311:289–326, 1996.

[11] T. Hirata, T. Kikuchi, T. Tsukada, and M. Hozawa. Finite element analysis of electrohydrodynamic time-dependent deformation of dielectric drop under uniform dc electric field. *J. Chem. Eng. Jpn.*, 33(1):160–167, 2000.

[12] S. K. Cho, H. J. Moon, and C. J. Kim. Creating, transporting, cutting, and merging liquid droplets by electrowetting-based actuation for digital microfluidic circuits. *J. Microelectromech. Syst.*, 12(1):70–80, 2003.

[13] J. A. Schwartz, J. V. Vykoukal, and P. R. C. Gascoyne. Droplet-based chemistry on a programmable micro-chip. *Lab on a Chip*, 4(1):11–17, 2004.

[14] D. L. Whitaker, C. Kim, C. L. Vicente, M. A. Weilert, H. J. Maris, and G. M. Seidel. Shape oscillations in levitated he ii drops. *J. Low Temp. Phys.*, 113:491–499, 1998.

[15] Lennart Ljung. *System Identification - Theory for the User*. Prentice Hall, 2nd edition, 1999.

[16] COMSOL AB. *FEMLAB Reference Manual*, 2002. Version 2.3.

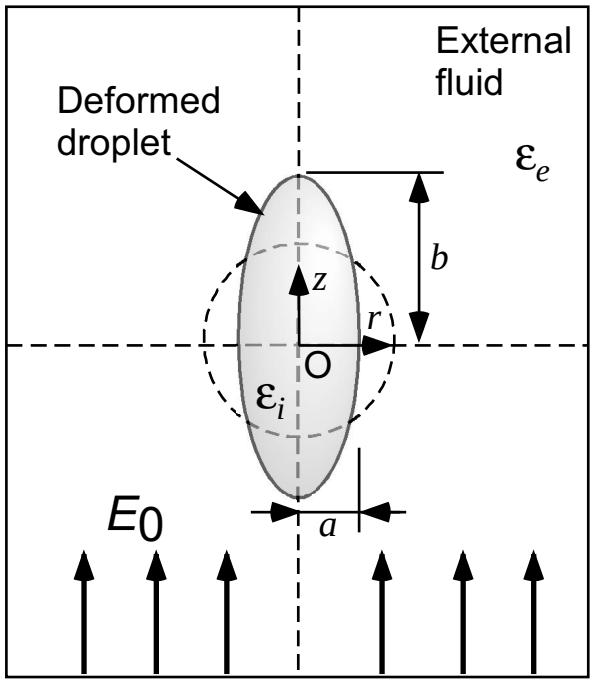


Figure 1: Schematic representation of the deformation of a droplet suspended in a second fluid in the presence of an electric field, $E_0$. The dashed circle represents the spherical shape of the non-deformed droplet. The cylindrical coordinate system used in the simulations is also shown.

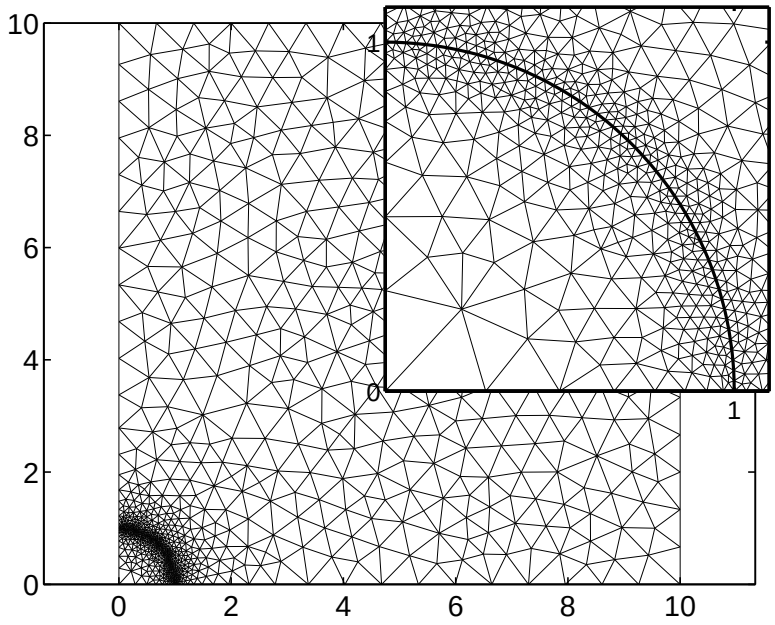


Figure 2: Typical meshed geometry for fluid problem. Dimensions are scaled with respect to the drop radius. The inset shows the details of the mesh near the droplet boundary.

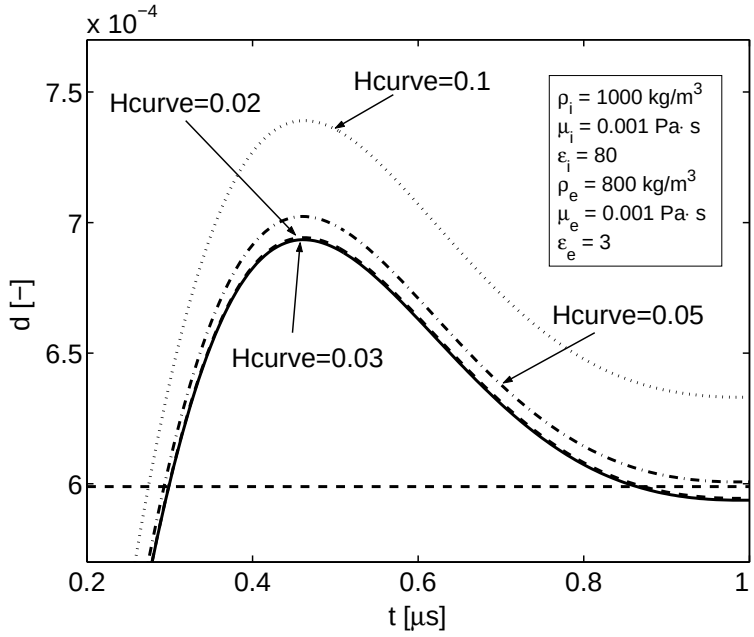


Figure 3: Convergence testing with mesh refinement using the refinement parameter `hcurve` in the fluid mechanics problem for an applied electric field of 1 MV/m and an interfacial tension of 20 mJ/m$^2$. Other parameters are shown in the legend.

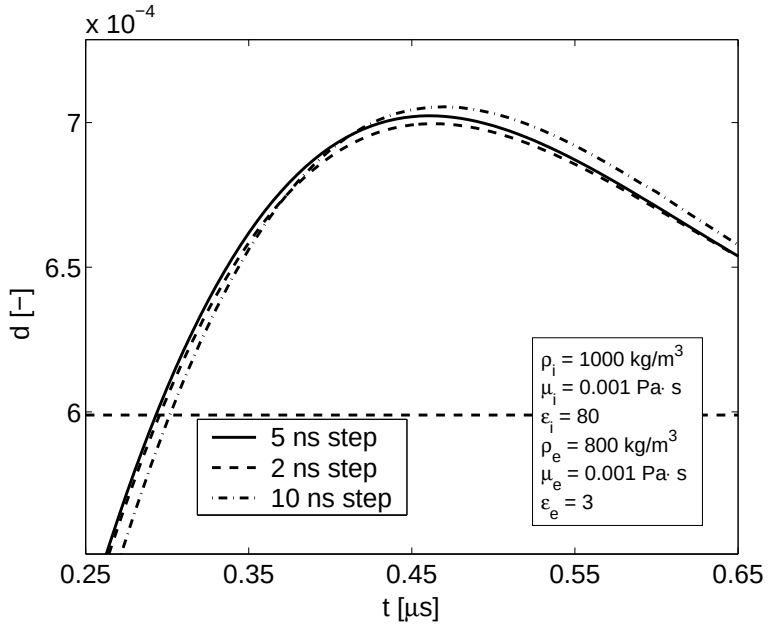


Figure 4: Convergence testing with time step refinement. All parameters are the same as in Figure 3.

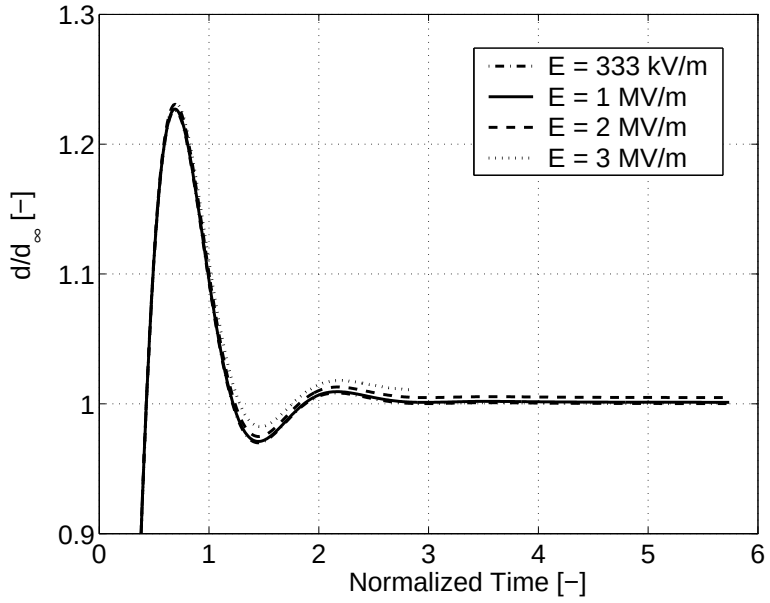


Figure 5: Variation of the scaled deformation of the droplet with scaled time for different applied field strengths. All other simulation parameters are provided in Table 1.

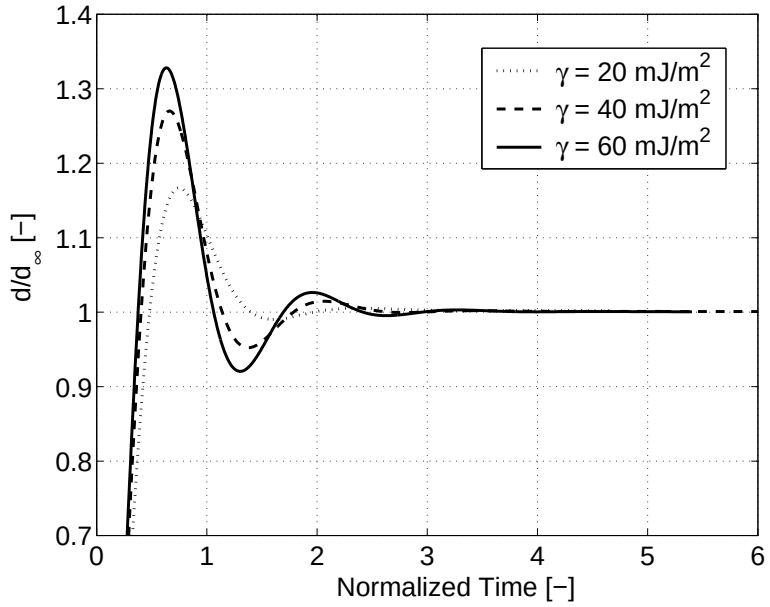


Figure 6: Dependence of the dynamic deformation of the droplet on interfacial tension. Other parameters as in Table 1

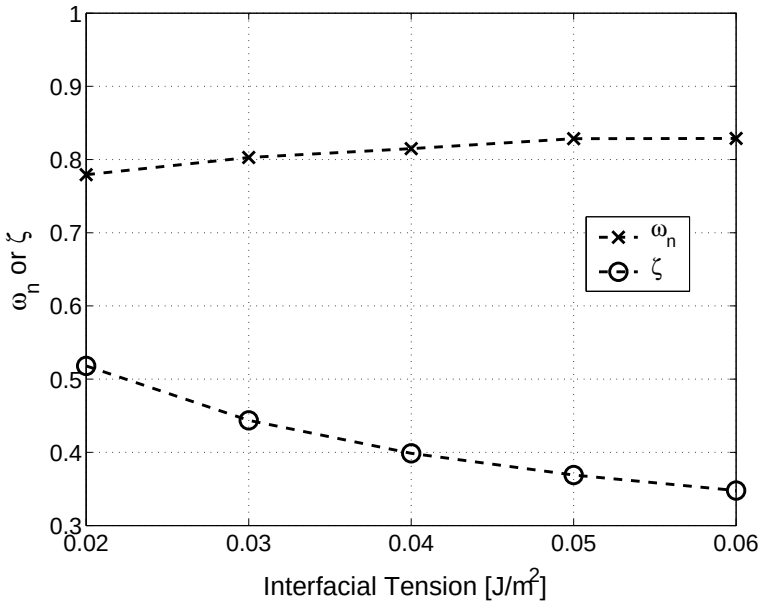


Figure 7: Variation of the natural frequency $\omega_n$ and damping ratio $\zeta$ with interfacial tension obtained from the LP model of the results in Figure 6.

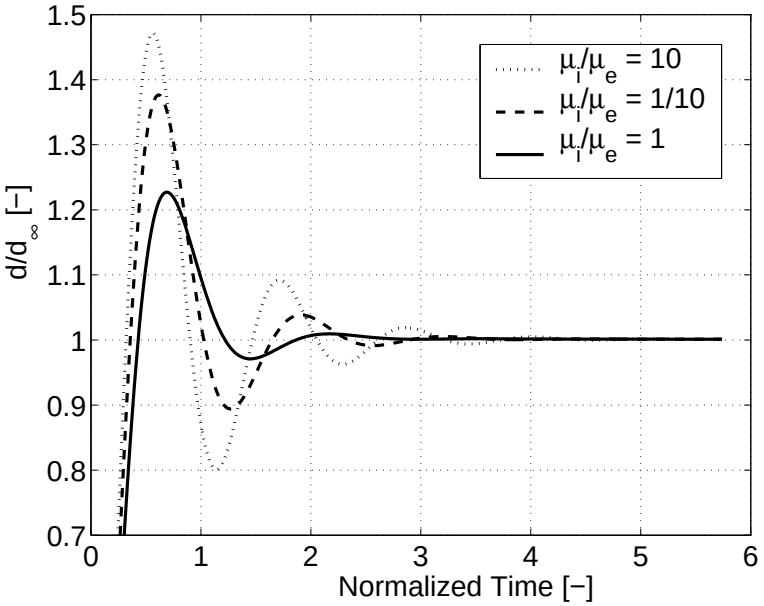


Figure 8: Dependence of the dynamic deformation on viscosity ratio. The simulations were performed using a maximum viscosity of 0.001 Pa·s (see text for details). Other parameters are given in Table 1.

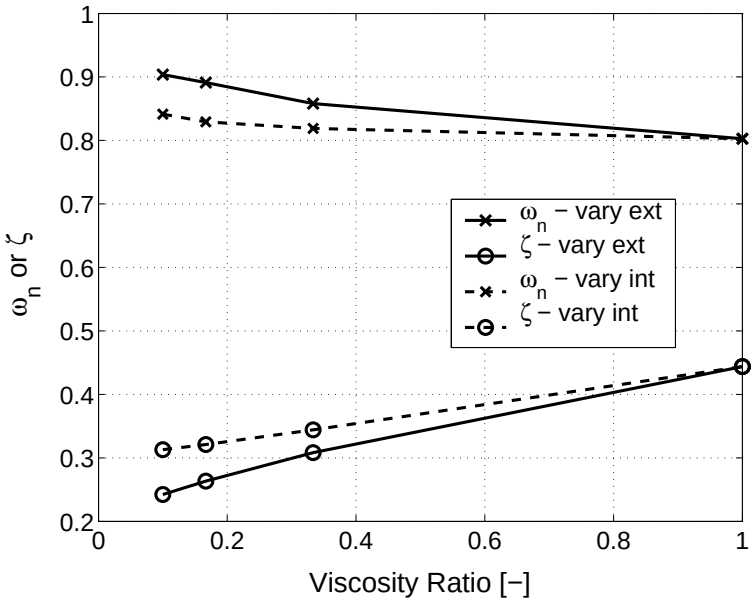


Figure 9: Variation of the natural frequency $\omega_n$ and damping ratio $\zeta$ with viscosity ratio obtained from the LP model of the results in Figure 8.

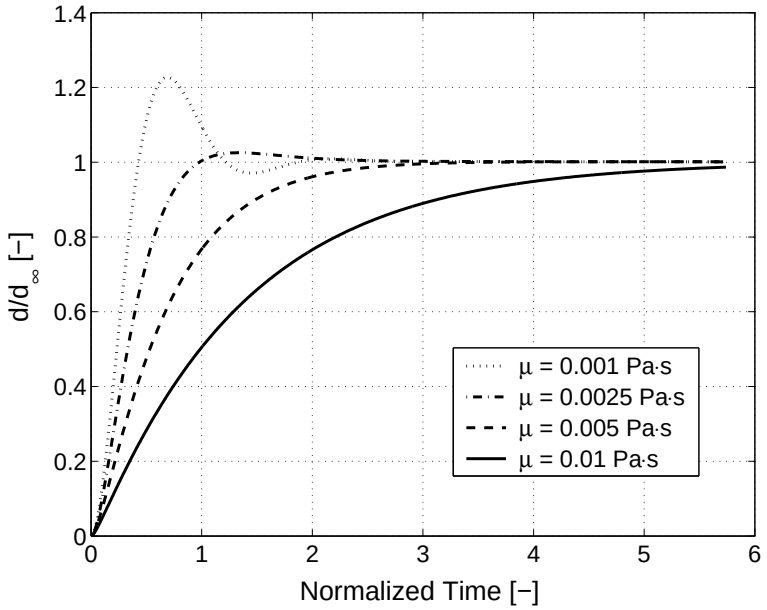


Figure 10: Dependence of the dynamic response of the droplet on viscosity of the fluids. The simulations were performed by keeping the viscosity ratio 1.

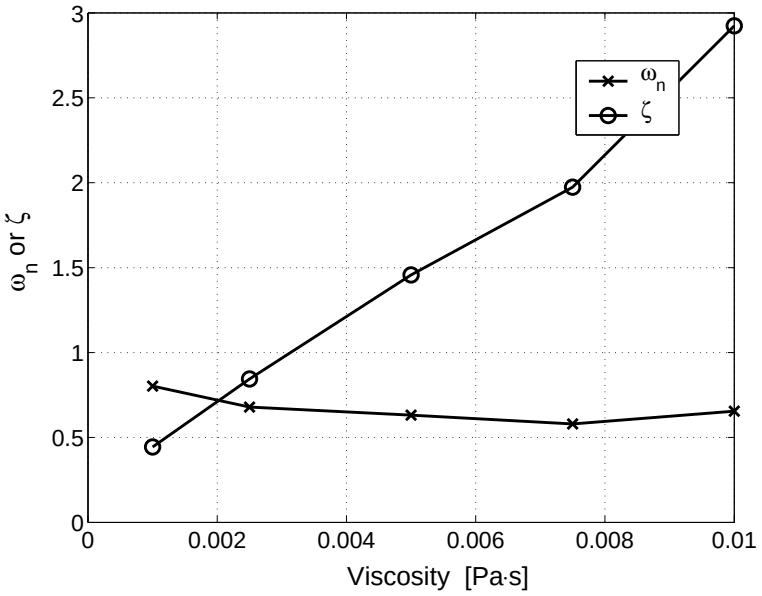


Figure 11: Variation of the natural frequency $\omega_n$ and damping ratio $\zeta$ with the magnitude of the viscosity obtained from the LP model of the results in Figure 10.